Vortex breakdown state selection as a meta-stable process

A. J. Fitzgerald* K. Hourigan* M. C. Thompson*

(Received 13 December 2004, revised 3 March 2005)

Abstract

Previous studies of unconfined swirling jets showed that both bubble and conical states of vortex breakdown can occur over a range of Reynolds numbers. State selection was postulated to be metastable, with small changes to initial conditions causing a discontinuous change to the final state for a particular final Reynolds-swirl number pair. Axisymmetric numerical simulations using a spectral element method of a swirling jet started from zero initial flow conditions show that the bubble state prevails at lower swirl ratios while the cone state dominates at higher swirl ratios. However, simulations where the jet evolution was started from a developed bubble state maintained that same state well into the region where previous simulations resulted

*Fluids Laboratories for Aeronautical and Industrial Research, Department of Mechanical Engineering, Monash University, Clayton, Australia.
mailto:aran.fitzgerald@eng.monash.edu.au

See http://anziamj.austms.org.au/V46/CTAC2004/Fitz for this article, © Austral. Mathematical Soc. 2005. Published May 15, 2005. ISSN 1446-8735

in conical breakdown. These results give some indication of the inherent stability of the bubble state relative to the cone state. They also extend the work of Billant, Chomaz, and Huerre [*J. Fluid Mech.*, 376:183–219, 1998] who observed the cone state from startup at swirl ratios slightly greater than the critical swirl ratio. In these simulations, perturbations cause the cone to be swept downstream only reappearing as a bubble with favourable perturbations.

Contents

1 Introduction

Vortex cores can be affected over a wide range of flow parameters by a flow phenomenon known as *vortex breakdown*. Vortex breakdown physics is important to flows in mixing vessels [4], meteorological phenomena (for example, tornados) [1], military [11] and civil aviation [10], and combustion [12]. In many cases, positive control of vortex breakdown yields improved characteristics of the base flows. Some examples of improved characteristics are: better flame holding and stability of a burner, and improved performance of military aircraft at high angles of attack.

Three main vortex breakdown topologies have been identified [5]: the bubble, spiral and double helix. Recently, a new type has been added to this list, designated *conical breakdown* due to its conical (near) axisymmetric expansion about the vortex core [3]. Find further details of vortex breakdown in recent review articles such as Lucca–Negro and O'Doherty [9].

Considerable research effort has been directed at discovering the existence of any universal critical parameters with the main aim of predicting the onset of vortex breakdown. These include parameters based on axial and azimuthal velocities such as the Rossby number [14], and parameters formed from the axial and azimuthal momenta [6]. These parameters are usually found for the whole vortex core at a location upstream of the vortex breakdown location, whereas another parameter, named the swirl angle, utilises local values of velocity at particular radial positions in the vortex core. Exceeding critical values of these parameters can indicate the onset of vortex breakdown. Recently, the swirl ratio $S = 2W/U$, where W and U are the peak azimuthal and axial velocities respectively, has been shown to fix the critical swirl ratio for vortex breakdown inception to $S_c \approx 1.4$ for $300 < \mathrm{Re} < 1200$ [3].

Benjamin [2] suggested that the essential mechanism of vortex breakdown is steady and axisymmetric. This hypothesis was later supported by numerical simulations of Grabowski and Berger [7], and later by Ruith et al. [13] where axisymmetric simulations were seen to capture the main flow topologies. However, this is not to say that vortex breakdown is purely axisymmetric at onset. Kurosaka et al. [8] used external disturbances to effect a vortex breakdown state change: a device was used to create azimuthally propagating disturbances in a standard diverging pipe flow, successfully altering the breakdown state from bubble to spiral and vice versa. Swirling jet experiments, involving weak (near the critical swirl ratio) bubble and cone states, have shown that perturbation of the flow usually leads to suppression of vortex breakdown [3]. The bubble state reappeared when more favourable perturbations were applied. In the experiments displaying cone vortex breakdown, a suppressed cone never reappeared with similar favourable perturba-

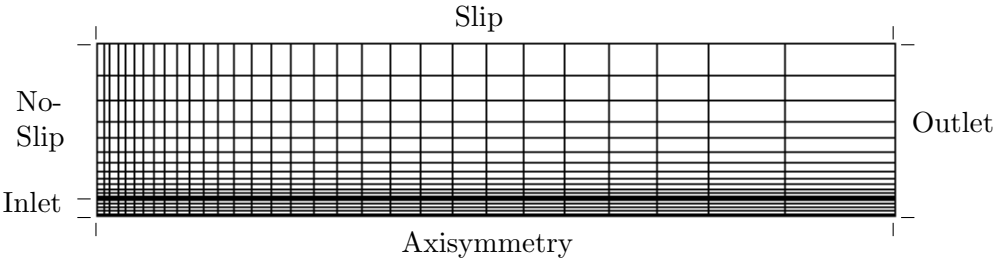

FIGURE 1: Computational mesh used in the simulations showing only the macro mesh elements and the location of the boundary types.

tions; however, a small transient bubble was often formed.

The key aims of this research were to determine if the selection of the final vortex breakdown state is dependent on the initial flow field conditions; and if this is true, to quantify the hysteresis of the selected state in terms of Reynolds and swirl numbers.

2 Numerical method

Axisymmetric numerical simulations of the Navier–Stokes equations were performed using a spectral element code developed and validated by Thompson, Leweke and Provansal [15]. The method employs high-order tensor product Lagrangian polynomials as shape functions within the discretisation elements. Accurate and efficient integration over each element is achieved by matching the node points of the Lagrangian polynomials to the Gauss–Legendre–Lobatto quadrature points. The method is second order accurate in time.

The computational grid used for the current set of simulations employs a structured mesh as shown in Figure 1. It has six *macro*-elements across the

jet inlet with mesh compression towards the nozzle outer radius R, to resolve the jet shear layer. The nozzle is located in the bottom left hand corner of the grid and covers 10% of the left boundary. There are thirteen macro-elements expanding out from the nozzle radius to the outer radial boundary at $r = 10R$. The axial domain length is $l = 46R$ and there are thirty macro-elements that expand away from the nozzle. The number of internal nodes within each macro-element was fixed for all cases at 36 (6×6), limiting the error in flow field characteristics, such as Strouhal number and point velocities, to better than 3%. This error estimate was determined through a series of simulations with higher numbers of internal nodes per element. At the inflow boundary the axial and azimuthal velocity profiles were specified, as shown in Figure 2. At the outlet boundary the normal components of velocity were set to zero. Recirculation at the outlet was prevented by the use of a *viscous sponge* region of very high relative viscosity. A free-slip condition was specified at the outer wall. The flow was evolved until it reached either a steady, periodic or non-periodic asymptotic state (dependent on flow parameters). Typically this involved 1–2 $\times 10^5$ timesteps.

In order to validate the results against a previous study, the axial and azimuthal velocity profiles given at the inlet were matched to the $S = 1.33$ profiles shown in Figure 4 of Billant et al. [3]. The profile for $S = 1.33$ was chosen as that was the closest swirl ratio to vortex breakdown onset. The actual profiles used can be seen in Figure 2, where the axial velocity profile is given above the axis of symmetry, and the azimuthal profile is given below for clarity. The axial $U(r)$ and azimuthal $W(r)$ profiles shown are scaled with the maximum axial velocity and the maximum azimuthal velocity, respectively. These profiles are derived by fitting eighth- and sixth-order polynomials for the axial and azimuthal data, respectively. For comparison purposes, the data extracted from Billant et al. are overlaid as points. The radial velocity V was set to zero at the inlet. The Reynolds number $\mathrm{Re} = 2R\bar{U}/\nu$, where $\bar{U}$ is the mass-flow averaged axial velocity.

To determine the metastability of the cone–bubble transition, it was nec-

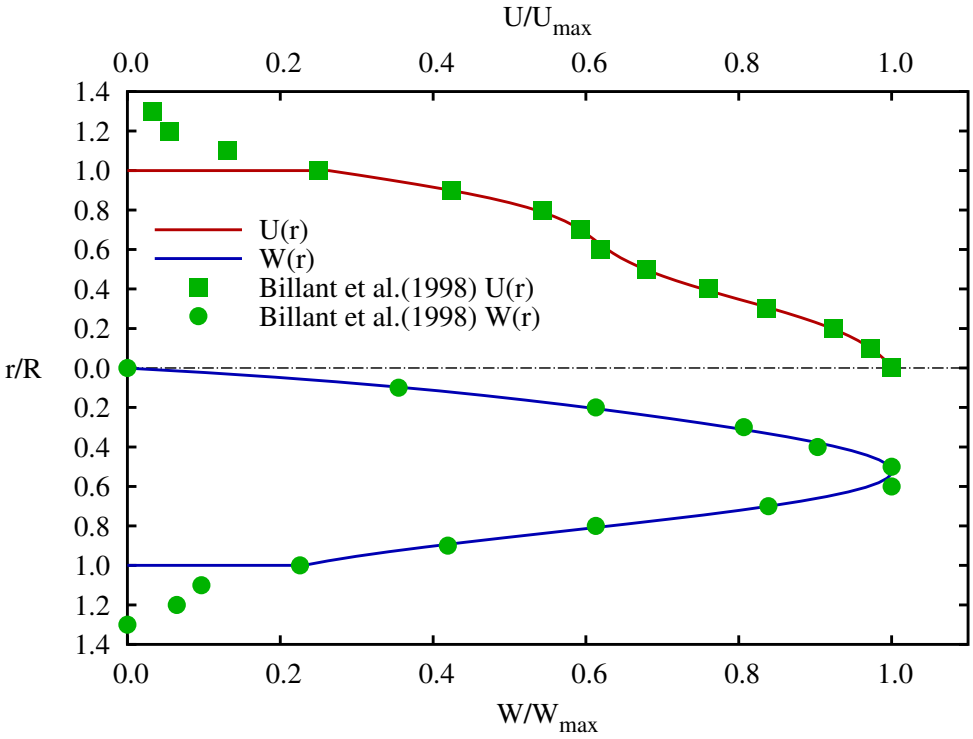

FIGURE 2: Velocity profiles used in all simulations, showing the data of Billant et al., (at Re = 1.33) in green squares and circles [3], and the polynomial fits used in these simulations. The Azimuthal (W) profile is given below $r/R = 0$, for clarity.

essary to create a map of the vortex breakdown states in Re–S parameter space. This was accomplished by running a series of time-accurate simulations starting from stationary initial flow at increasing swirl ratios, with sufficient resolution such that the critical swirl ratio S_c could be determined to within $S \pm 0.02$. This was done for a range of Reynolds numbers. Secondly, five Re–S pairs where chosen such that the vortex breakdown state was a steady bubble. From these five locations on the parameter map, three paths with increasing S and three paths with increasing Re were chosen such that they passed through the bubble–cone transition line and well into the cone dominated region. Simulations were run by restarting the flow with the bubble state and increasing the given parameter in steps. Each step was left to develop for 1×10^5 timesteps before checking the final breakdown state.

3 Results and discussion

Qualitative results show that both the bubble and the cone state are achieved with the numerical method used. The axisymmetric condition allows not only a steady bubble and cone state, but also the unsteady cases seen in the literature [3]. Most importantly, the unsteady three-dimensional behaviour found in experimental cone breakdown is replicated in an axisymmetric form, as seen in Figure 3, and the simulations have the same time-dependent roll-up and shedding behaviour seen by Billant et al. [3] in their experiments. This result is important to show that the axisymmetric simulations reproduce the essential breakdown types. In addition, the swirl ratios for the onset of breakdown match the experimentally-determined values to $\Delta S_c \leq 2\%$ for $500 \leq \mathrm{Re} \leq 1000$.

Figure 4 upper, shows the results of an extensive parametric study of the simulated swirling jet. Each point represents an individual simulation, where the Reynolds number was chosen and a variety of swirl ratios were tested to determine the final vortex breakdown state for those parameters.

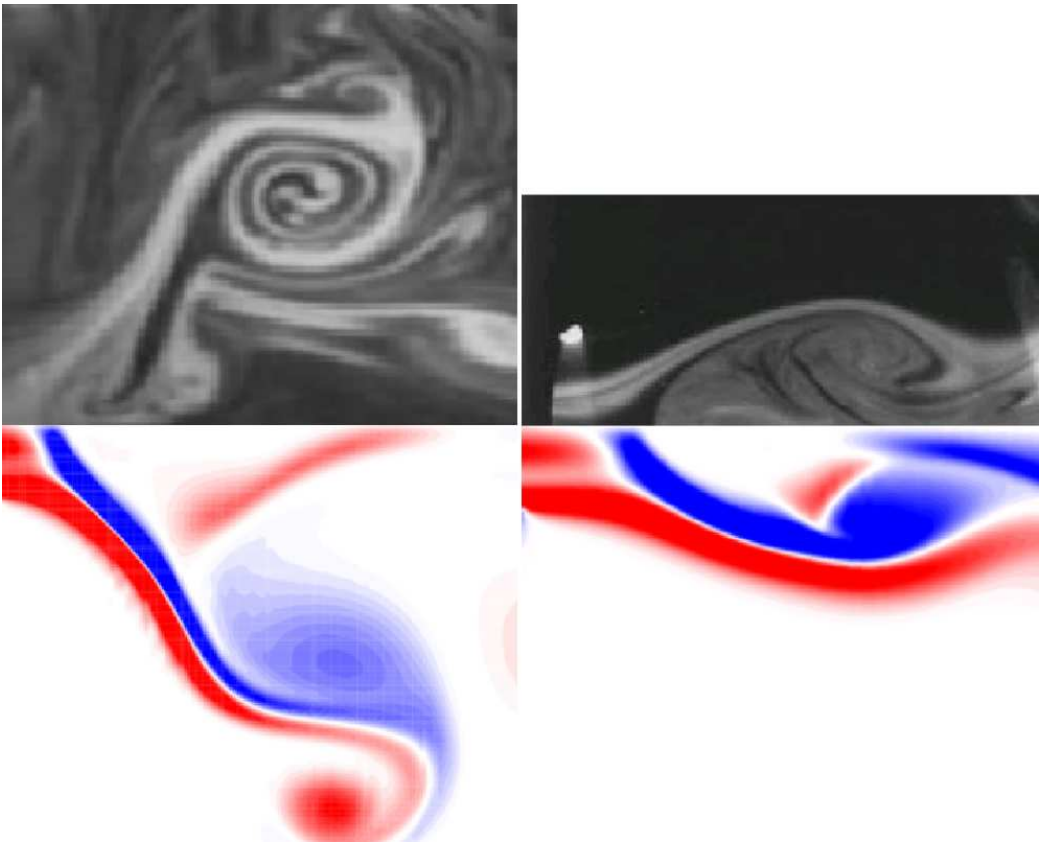

FIGURE 3: Qualitative comparisons between contours of azimuthal vorticity from the present simulations (lower half) and dye visualisations by Billant et al. [3], at $\mathrm{Re} \approx 600$, $S \approx 1.4$. Left shows unsteady conical vortex breakdown and right shows near-steady bubble vortex breakdown

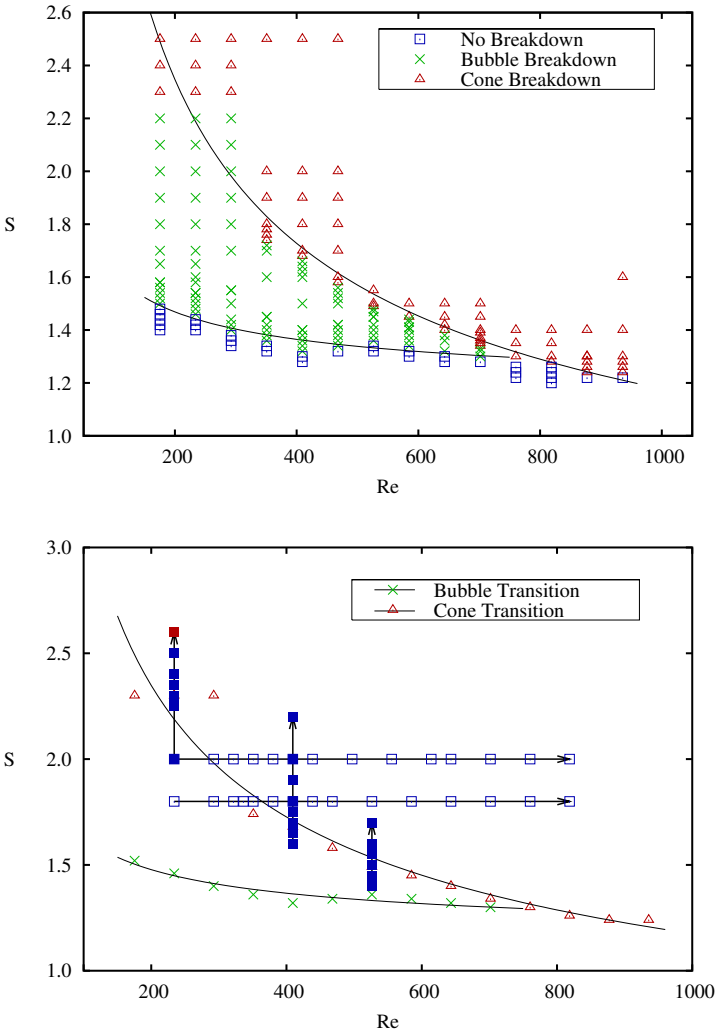

FIGURE 4: Results of independent Re–S pair simulations showing definition lines between no-breakdown, bubble breakdown and cone breakdown types (above). Results of increasing the S and Re parameters from four strong bubbles, into the cone breakdown region (below). In most cases, the transition to the cone type vortex breakdown was completely suppressed.

This process was performed for the Reynolds number range of $150 \lesssim \mathrm{Re} \lesssim 950$ with steps of $\mathrm{Re} \approx 60$. The results show that below a critical swirl ratio S_c, the jet experiences no vortex breakdown, represented by the blue squares. Closer analysis of the axial velocity along the jet centreline shows that when approaching S_c, a significant velocity defect is apparent. For Reynolds numbers up to $\mathrm{Re} \approx 750$, increases in the jet swirl ratio cause vortex breakdown of the bubble type to appear in the vortex core. For these Reynolds numbers, a further increase in swirl ratio, above a transition swirl ratio S_t, causes vortex breakdown of the cone type exclusively. For the range $750 \lesssim \mathrm{Re} \lesssim 950$, the bubble state was not reliably experienced. Instead, increases in the swirl ratio to above S_c were found to cause vortex breakdown of the cone type almost exclusively.

The critical swirl ratio S_c is almost Reynolds number independent as seen in both the results of Billant et al. [3] and the present results, except at low Reynolds numbers where viscosity plays a minor role. More significant Reynolds number dependence is evident in the transition swirl ratio S_t, where a significantly higher swirl ratio is required at low Reynolds numbers to cause cone-type vortex breakdown. This relationship indicates that viscosity is important in the vortex breakdown state-selection process.

Figure 4 lower, shows the lines and data that define the critical swirl ratio and transition swirl ratios on the same parameter space as Figure 4 upper. Superimposed on this map are the results from the metastability tests, indicated by solid and hollow symbols with arrows. These show the starting Re–S pair and the breakdown type at each stage of the simulation.

In the case of the three tests indicated by solid symbols, the swirl ratio was increased by increasing the azimuthal velocity while maintaining the initial Reynolds number. In all three cases, an increase in the swirl ratio, well into the region where cone vortex breakdown is expected, yielded no change in the vortex breakdown state from a bubble. In the case of the simulation run from $\mathrm{Re} \approx 230$ and $S = 2.00$, the cone state was finally achieved at $S \approx 2.7$, indicated by the solid red square. This swirl ratio is significantly

above $S = 2.3$ where the cone became evident in the first set of simulations. The other two cases were not stepped forward sufficiently to obtain cone breakdown states.

The breakdown states denoted by the open symbols were achieved by increasing the Reynolds number while maintaining the swirl ratio. As with the previous set of simulations, the bubble is maintained while increasing the swirl ratio well into the cone-breakdown region. In the case starting at $\mathrm{Re} = 400$ and $S = 1.5$, numerical convergence difficulties were encountered preventing the simulations from extending into the cone vortex breakdown region. This data has subsequently been left out of the plot. In the remaining two cases, the cone state was not achieved even though the bubble had significantly enlarged and was beginning to become unstable.

The observations described above give a picture of a very stable bubble form that resists opening into a cone when the Reynolds or swirl number are slowly increased quasi-statically. A cone type of vortex breakdown is more likely to occur at lower values of the critical parameters when the perturbation from the jet starting vortex is felt. Once the cone is established it has been seen to be reasonably stable. However, some simulations have shown the opening and closing of the cone state to tend towards reforming a bubble. As yet, simulations have only shown transient cones becoming bubbles at lower swirl ratios.

4 Conclusions

Axisymmetric numerical simulations using the spectral element method are able to capture the major features of the equivalent experiments including the vortex breakdown types. The unsteady behaviour of the three-dimensional cone breakdown type was also seen in the axisymmetric model to a reasonable qualitative degree. The model was also validated by replication of the critical swirl ratios found by Billant et al. [3] to within a few percent.

For a jet starting from zero flow conditions at a particular Re–S pair, a full parameter map was generated, showing the regions where no-breakdown, bubble breakdown and cone breakdown occurred. Five sets of simulations, where either Re or S were gradually increased, were used to investigate the metastability of different breakdown types. Results of these tests showed that the bubble vortex breakdown state can persist well into the cone breakdown region.

Simulations that are started from zero initial conditions show a preference for the development of the cone-type of vortex breakdown at substantially lower swirl ratios than if the cone state is approached by passing through a stable bubble stage. Presumably the large perturbations involved in the starting jets (including the presence of a strong starting vortex ring) can allow the cone vortex breakdown to appear. This finding corresponds well with the findings of Billant et al. [3], where perturbations on a weak cone vortex breakdown caused the complete destruction of the cone vortex breakdown. Additionally, these vortex cores were never able to regain the cone vortex breakdown state, but were seen to reform a transient bubble.

Acknowledgment: Mr. Fitzgerald acknowledges the support of the Department of Mechanical Engineering, Monash University, through a Departmental Scholarship.

References

[1] W. Althaus, C. Brücker, and M. Weimer. Breakdown of slender vortices. In *Fluid Vortices* (ed. S. Green), pages 373–426, 1995. C352

[2] B. T. Benjamin. Theory of the vortex breakdown phenomenon. *J. Fluid Mech.*, 14(4):593–629, 1962. C353

[3] P. Billant, J.-M. Chomaz, and P. Huerre. Experimental study of vortex breakdown in swirling jets. *J. Fluid Mech.*, 376:183–219, 1998. C353, C355, C356, C357, C358, C360, C361, C362

[4] M. P. Escudier. Observations of the flow produced in a cylindrical container by a rotating endwall. *Exps. Fluids*, 2:189–196, 1994. C352

[5] J. H. Faler and S. Leibovich. An experimental map of the internal structure of a vortex breakdown. *J. Fluid Mech.*, 86:313–335, 1978. C353

[6] S. Farokhi, R. Taghavi, and E. J. Rice. Effect of initial swirl distribution on the evolution of a turbulent jet. *AIAA Journal*, 27(6):700–706, 1988. C353

[7] W. J. Grabowski and S. A. Berger. Solutions of the navier-stokes equations for vortex breakdown. *J. Fluid Mech.*, 75:525–544, 1976. C353

[8] M. Kurosaka, Kikuchi M., K. Hirano, T. Yuge, and H. Inoue. Interchangeability of vortex-breakdown types. *Exps. Fluids*, 34:77–86, 2003. C353

[9] O. Lucca-Negro and T. O'Doherty. Vortex breakdown: A review. *Prog. Energy Combust. Sci.*, 27:431–481, 2001. C353

[10] A. Mager. Dissipation and breakdown of a wing-tip vortex. *J. Fluid Mech.*, 55(4):609–628, 1972. C352

[11] M. Özgören, B. Sahin, and D. Rockwell. Vortex structure on a delta wing at high angle of attack. *AIAA Journal*, 40:258–292, 2002. C352

[12] J. Panda and G. K. McLaughlin. Experiments on the instabilities of a swirling jet. *Phys. Fluids*, 6:262–276, 1994. C352

[13] M. R. Ruith, P. Chen, E. Meiburg, and T. Maxworthy. Three-dimensional vortex breakdown in swirling jets and wakes: Direct numerical simulation. *J. Fluid Mech.*, 486:331–378, 2003. C353

[14] R. E. Spall, T. B. Gatski, and C. E. Grosch. A criterion for vortex breakdown. *Phys. Fluids*, 30(11):3434–3440, 1987. C353

[15] M. C. Thompson, T. Leweke, and M. Provansal. Kinematics and dynamics of sphere wake transition. *J. Fluids Structures*, 15:575–585, 2001. C354